Separation and Purification Technology 163 (2016) 341–351

Contents lists available at ScienceDirect

Separation and Purification Technology

journal homepage: www.elsevier.com/locate/seppur

Predicting equivalent settling area factor in hydrocyclones; a method for determining tangential velocity profile

Reza Sabbagh [a], Michael G. Lipsett [b], Charles R. Koch [b], David S. Nobes [a,*]

[a] Optical Diagnostics Group, Department of Mechanical Engineering, University of Alberta, Edmonton, Alberta T6G 2G8, Canada
[b] The Department of Mechanical Engineering, University of Alberta, Edmonton, Alberta T6G 2G8, Canada

ARTICLE INFO

Article history:
Received 4 June 2015
Received in revised form 21 January 2016
Accepted 7 March 2016
Available online 9 March 2016

2010 MSC:
00-01
99-00

Keywords:
Hydrocyclone
Equivalent settling area
Performance
Centrifugal separation
Tangential velocity

ABSTRACT

Predicting the equivalent settling area of the hydrocyclones is important for selection and design of the device. It also allows comparison of hydrocyclone to other separators that work using a similar concept. A mathematical model based on the physics of the separation phenomenon in the hydrocyclone is developed to predict the equivalent area factor of the hydrocyclone. The effect of the overflow and inlet diameters on the hydrocyclone performance are evaluated and it is shown that changing the overflow diameter has more effect on the equivalent area factor than the inlet diameter. The equivalent settling area model (ESAM) is validated with experimental data from experiments using a 50 mm diameter hydrocyclone and glass bead particles. Good agreement between ESAM and the experiments is observed. An advantage of ESAM is that it can be used to estimate the tangential velocity profile in a hydrocyclone. A method of predicting the tangential velocity profile on the basis of equivalent settling area without performing velocity measurement is detailed and examined for an experimental velocity profile. This allows the ESAM to be used as a framework for design of the hydrocyclone devices.

1. Introduction

Physical separation processes such as centrifugal separators have many applications in industry [1,2]. However, a model to predict the performance of a device for comparison to other devices is essential during design and for scaling up the separator. One method for modeling the performance of the centrifuge separators compares the settling area of a continuous flow gravity settling tank with the settling area of a tank that has the same performance as that of a centrifuge device with a rotary wall [3,4]. This surface area of the imaginary gravity settling tank is called the equivalent settling area (also known as equivalent area factor or capacity factor) of the separator.

A hydrocyclone is considered to be a centrifugal separator with a fixed wall. The centrifuge force is generated from the tangential injection of the flow into the hydrocyclone. Interaction with the wall turns the flow, creating centrifugal acceleration force which drives the separation of the particles from the liquid.

To understand the swirling flow in the hydrocyclone, the flow pattern has been investigated through experimental measurements of velocity components [5–10]. In addition, models have been developed to predict the hydrocyclone behavior [11–20]. These include empirical models [21,15,16,22], analytically developed models on the basis of physics of flow in the hydrocyclone [11–13,17,23,19] and more often, numerical models [24–26]. Review of such studies can be found in [27,28,24,29]. Although models have been developed to predict the performance of the hydrocyclones, these models are not in a form that allows direct comparison with other types of centrifugal separators.

Equivalent settling area is a concept used to compare the performance and scaling up of different centrifugal separators [30,31]. For hydrocyclones, [32] discussed the importance of the performance in terms of the equivalent area and indicated that there is limited available information for developing the equivalent area. A mathematical model to obtain the equivalent area of the device is lacking although some works has been done to predict the performance region of the hydrocyclones based on equivalent settling area using both experiments and mathematical modeling [33].

In this paper, a mathematical approach to develop equivalent settling area model (ESAM) is presented to predict the performance

* Corresponding author at: Optical Diagnostics Group, Mechanical Engineering Department, University of Alberta, Edmonton, Alberta, Canada.
E-mail address: david.nobes@ualberta.ca (D.S. Nobes).

http://dx.doi.org/10.1016/j.seppur.2016.03.009
1383-5866/

of the hydrocyclone using a similar technique to other centrifugal separators. Background theory is discussed first and then the derivation of the ESAM is detailed. The experimental procedure for validating the ESAM is explained and results from the experiments are used to validate the ESAM. Four different types of hydrocyclone designs are studied for model validation. The effect of design parameters on the hydrocyclone performance is detailed and examined using the experimental results. The advantage of using the ESAM in flow prediction without performing a flow measurement is discussed. The ability of the ESAM in providing a quantifiable information for predicting the equivalent settling area factor is also investigated over broad ranges of design and operating conditions.

2. Modeling

2.1. Basic concepts

In developing the equivalent settling area of a centrifuge (i.e. the area of a continuous gravity settling tank that has the same performance as the centrifuge) a 50% cut size particle is assumed to be separated in the centrifuge during its stay in the device. This is a similar concept to residence time theory which assumes that a 50% cut size particle will be separated in a hydrocyclone during the residence time if it reaches the hydrocyclone wall when the particle is injected into the hydrocyclone exactly from the middle of the inlet section pipe [34]. The assumptions used for the residence time concept are the basis for developing an equivalent area for centrifugal devices [4]. Combining residence time theory with the assumptions of Stokes' law [35], the radial velocity due to the centrifugal acceleration is [34]:

$$v_r = \frac{\Delta\rho d^2}{18\mu}\frac{v_\theta^2}{r} \tag{1}$$

where d is the particle diameter, $\Delta\rho$ is density difference between phases, μ is dynamic viscosity of the fluid and the term v_θ^2/r is the centrifugal acceleration where v_θ is the tangential velocity component and r is the radius of the rotation. The radial velocity v_r can be related to the vertical velocity (v_z) using the chain rule. Assuming that the flow near the hydrocyclone wall follows the shape of the wall [34], v_r is approximated by:

$$v_r = \frac{dr}{dt} = \frac{dr}{dz}\frac{dz}{dt} = \frac{D}{2L}v_z \tag{2}$$

where dr and dz are line elements in the radial and vertical directions, dt is the time element, D is the hydrocyclone diameter and L is the total length as defined in Fig. 1.

In the residence time theory [12,34], the ratio of the axial velocity to the inlet velocity is assumed to be constant. This has been discussed in detail in [36,12]. The constant velocity ratio results in simplifying the axial velocity to take a constant value in a hydrocyclone. This simplification is used in developing the current model to estimate the axial velocity. Assuming the vertical velocity of the particle equals that of the liquid [12], the vertical velocity component can be estimated from the inlet flow rate Q in the hydrocyclone cylindrical section region between the hydrocyclone wall and the vortex finder:

$$v_z = \frac{4Q}{\pi(D^2 - D_o^2)} \tag{3}$$

where D_o is the overflow diameter. The flow rate can be obtained using Eq. (3) combining with Eqs. (1) and (2):

$$Q = \frac{\Delta\rho d^2}{9\mu}\frac{\pi(D^2 - D_o^2)L}{4D}\frac{v_\theta^2}{r} \tag{4}$$

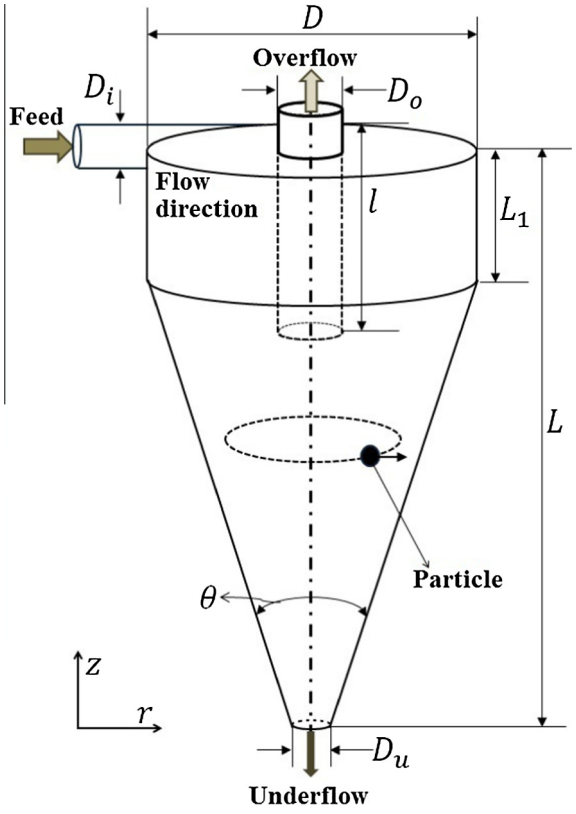

Fig. 1. A schematic of a hydrocyclone showing basic components and operation principles.

which can be simplified to:

$$Q = 2v_g\frac{\pi(D^2 - D_o^2)L}{4gD}\frac{v_\theta^2}{r} \tag{5}$$

where v_g is settling velocity under gravitational acceleration (not under centrifugal acceleration) for 50% cut size particle where 50% of particles (by mass) which are larger (smaller) than this size pass through each of the outlets of the separator.

The gravitational settling velocity v_g is defined as:

$$v_g = \frac{\Delta\rho d^2}{18\mu}g \tag{6}$$

where d is the particle 50% cut size diameter and v_g is calculated using Stokes' law assuming that particles are fine enough to satisfy Stokes' law assumptions and travel at terminal velocity.

For hydrocyclones it has been experimentally found that v_θ is a function of r such that $v_\theta = C/r^n$ where the constant C and exponent n are typically determined from experiments [34]. The constant C can be obtained from a mass balance by integrating the tangential velocity at the inlet section area from r_1 to r_2 (for a rectangular inlet pipe $r_1 = D/2$ and $r_2 = D/2 - w$ where w is the inlet pipe width as defined in Fig. 2) and then equating to the feed volume flow rate [33]. Therefore, v_θ is obtained such that:

$$v_\theta = \frac{Q(1-n)}{H(r_2^{1-n} - r_1^{1-n})r^n} \tag{7}$$

where H is the depth of the rectangular inlet pipe defined in Fig. 2.

The tangential velocity component is also related to the pressure drop in the hydrocyclone. This is shown by considering the Navier–Stokes equation in cylindrical coordinates (r, θ, z) [35] for the radial direction as defined in Fig. 3 to be:

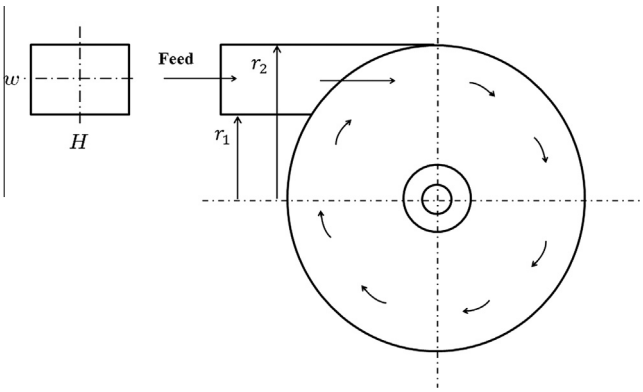

Fig. 2. Plan view of the cylindrical portion of the hydrocyclone with a rectangular inlet for defining model variables.

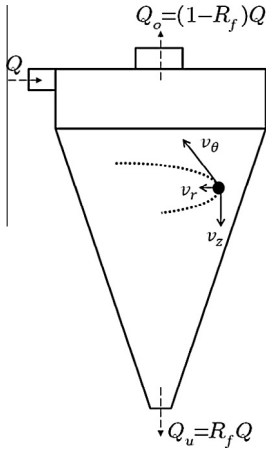

Fig. 3. Schematics of velocity components and flow rates in a hydrocyclone.

$$\frac{\partial v_r}{\partial t}+v_r\frac{\partial v_r}{\partial r}+\frac{v_\theta}{r}\frac{\partial v_r}{\partial \theta}+v_z\frac{\partial v_r}{\partial z}-\frac{v_\theta^2}{r} =\frac{-1}{\rho}\frac{\partial P}{\partial r} +\frac{\mu}{\rho}\left[\frac{\partial}{\partial r}\left(\frac{1}{r}\frac{\partial (r v_r)}{\partial r}\right)+\frac{1}{r^2}\frac{\partial^2 v_r}{\partial \theta^2}+\frac{\partial^2 v_r}{\partial z^2}-\frac{v_r}{r^2}-\frac{2}{r^2}\frac{\partial v_\theta}{\partial \theta}\right]+g_r \quad (8)$$

where t is time, P is pressure and g_r represents body forces. For a steady state flow and no gravity (body force) in the radial direction, the first and last terms of Eq. (8) are zero. Since the radial velocity in absolute terms is much smaller compared to the other velocity components [37,38], the terms including v_r and its derivatives are neglected, resulting in:

$$v_r\frac{\partial v_r}{\partial r}-\frac{v_\theta^2}{r}=\frac{-1}{\rho}\frac{\partial P}{\partial r}+\frac{\mu}{\rho}\left(-\frac{2}{r^2}\frac{\partial v_\theta}{\partial \theta}\right) \quad (9)$$

The tangential velocity v_θ is also a function of the radial position in the hydrocyclone as in Eq. (7) and hence its θ and z derivatives are zero. The following relation is then an expression for pressure changes within the hydrocyclone:

$$\frac{1}{\rho}\frac{\partial P}{\partial r}=\frac{v_\theta^2}{r} \quad (10)$$

This expression balances the pressure force with centrifugal acceleration per unit volume and indicates that the pressure increases toward the hydrocyclone wall as the centrifugal force increases.

The pressure drop (ΔP) in a hydrocyclone is obtained by using Eq. (10). Replacing v_θ from Eq. (7) and integrating it in the radial direction between the overflow radius ($D_o/2$) and hydrocyclone radius ($D/2$) results in:

$$\Delta P=\frac{2^{2n-1}\rho}{n}\left(\frac{Q(1-n)}{D^n H(r_2^{1-n}-r_1^{1-n})}\right)^2\left[\left(\frac{D}{D_o}\right)^{2n}-1\right] \quad (11)$$

At a known flow rate this gives the pressure drop for a hydrocyclone if the exponent n is known. A good approximation for the value of n is 0.8 [39] which can be used for majority of the hydrocyclones.

2.2. Equivalent area factor

In a continuous gravity settling tank separator, flow rate is proportional to gravitational settling velocity of particles [32], where the proportionality coefficient is the surface area of the tank. Similarly, assuming a uniform distribution of the particles in operation, for centrifuge separators [4] defined the equivalent area factor (also termed the theoretical capacity factor and is shown by Σ) with SI units of m^2 as:

$$\Sigma=\frac{Q}{2v_g} \quad (12)$$

For a centrifuge separator, $\Sigma=1$ shows that its performance equals to the performance of a gravity tank with surface area of 1 m^2 at the same flow rate. A higher value of Σ is desired as it is an indication of the separator performance.

To develop an equivalent area relation for hydrocyclones, the flow rate is related to centrifugal acceleration (Eq. (5)) and the equivalent area factor Σ is obtained by combining Eqs. (12), (7) and (5) and replacing Q^2 with the pressure drop relation from Eq. (11) resulting in:

$$\Sigma=\frac{\pi L n D^{2n+1}[1-(D_o/D)^2]\Delta P}{\rho g(D-w)^{2n+1}[(D/D_o)^{2n}-1)]} \quad (13)$$

where w the width of the rectangular shape inlet section equals r_2-r_1. Since the inlet section depth H does not appear in Eq. (13) for hydrocyclones with circular inlet pipes, by assuming $w=D_i$, the equivalent area is:

$$\Sigma=\beta\frac{L\Delta P}{\rho g} \quad (14)$$

where

$$\beta=\frac{\pi n[1-(D_o/D)^2]}{(D/D_o)^{2n}-1}\left(\frac{1}{1-D_i/D}\right)^{2n+1} \quad (15)$$

This relationship can also be used for other inlet section types. The equivalent diameter to a circular pipe can be used in Eq. (15) if obtained from equating the inlet section area to the area of a circular pipe. Mathematically Eq. (15) is held if the following conditions hold: $D_o/D>0, D_i/D<1$, and $D_o/D\neq 1$. All of theses criteria are satisfied in practice for a typical hydrocyclone. The impact of the incoming flow and the overflow pipe (the portion of the overflow pipe inside the hydrocyclone is called vortex finder) wall causes turbulence in the flow. To avoid this turbulence, $(2D_i/D+D_o/D)\leq 1$ can be considered as a limit for inlet pipe and the vortex finder diameters.

Eq. (15) indicates that for geometrically similar hydrocyclones, β depends on the value of n and the ratio of inlet (D_i) and overflow (D_o) diameters to hydrocyclone diameter (D). A hydrocyclone diameter could affect the value of β implicitly through the value of n, which could change the tangential velocity component [6]. However, it is believed that the value of n is independent of the

hydrocyclone size in most cases [40] and for this reason β is considered a useful design parameter.

In developing the ESAM, the assumptions of Stokes' law for calculating radial velocity of particles are used and it is also assumed that the interaction between particles is negligible. This requires a low concentration of solid particles in the feed flow. The value of volume solid concentration for unhindered settling varies from 1% to 11% for spherical particles [40,34]. For non-spherical particles this limit reduces to 4% [40]. At high solid concentration, particle–particle interactions reduce the settling velocity and hindered settling effects [41,42] are significant.

3. Experiments

3.1. Experimental apparatus

An experimental flow circuit has been designed and built as shown in Fig. 4 to validate the ESAM developed in (14) for predicting the equivalent settling area factor. Water with particles are pumped into the hydrocyclone using a centrifugal pump that provides different inlet flow rates and hence pressures. Pressure is monitored at the inlet and the outlets to obtain the pressure drop across the hydrocyclone. Pressure transducers (AST4000) with 4–20 mA outputs are calibrated according to ASTM D5720-95 [43] and used for pressure monitoring. The accuracy is ±0.4% for the best fit straight line (BFSL) and the measurement range is from zero to 200 kPa.

A second pump (a progressive cavity pump) is connected to the underflow pipe to allow independent control of the underflow flow rate without clogging the underflow pipe. This method has an advantage compared to using a valve for manipulating the underflow flow rate since a valve in the underflow pipe can easily block [34]. Another important feature of using a pump for the underflow is it provides the opportunity to simulate underflow diameter variation. Each pump is controlled using a separate variable frequency drive (VFD). Both underflow and overflow are returned to the tank for recycling. To keep the particles uniformly mixed and suspended during the experiment, an agitator mixes the particles in the tank.

Flow at the inlet and underflow are measured by coriolis flow meters (Promass 83I Endress+Hauser Ltd with maximum measurement error of ±0.05% for inlet flow; Optimass7300 KROHNE Messtechnik GmbH with maximum measurement error of ±0.1% of the actual measured flow ±0.0018 m^3/h for underflow). Using the coriolis meters, temperature, velocity, density and solid concentration are measured. Total volume of the flow in the system is 260 l and the experiments have been performed at the four particles volume concentrations of: 0.1%, 0.5%, 1% and 2% mixed with water as liquid. Liquid properties are determined according to its temperature measured in flow meter. The ratio of the volumetric underflow flow rate to the inlet flow rate (the flow ratio R_f as defined in Fig. 3) due to the underflow pumping varies from 0.2 to about 0.8. The experiments conditions are listed in Table 1.

Control of the experimental hardware (including pumps and mixer VFDs), communication with coriolis flow meters and record-

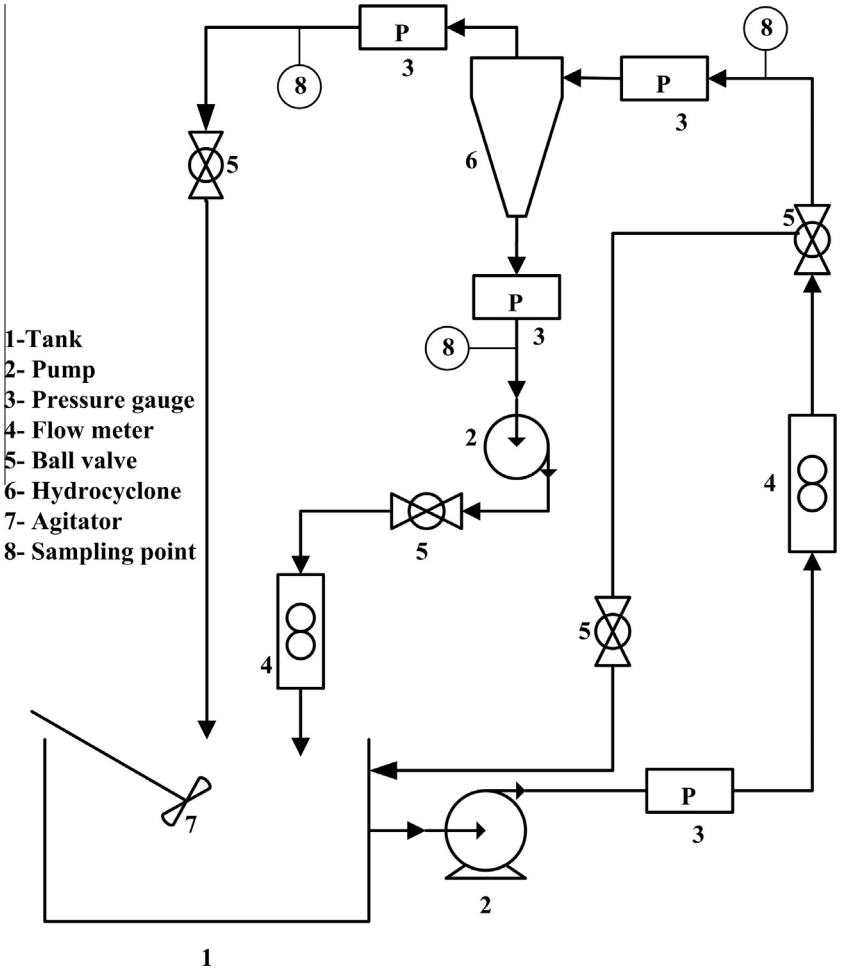

Fig. 4. Process flow diagram for the experimental setup.

Table 1
Experiments conditions.

Parameter	Condition
Centrifugal pump speed (Hz)	40, 50, 60
Underflow progressive cavity pump speed (Hz)	10–50
Inlet pressure (kPa)	150–230
Inlet flow rate (m^3/h)	1–2.4
Inlet solid volume concentration (%)	0.1–2

ing the data from the devices and temperature and pressure sensors is performed using custom software (LabWindows/CVI, National Instruments Corporation). At steady state flow conditions information is recorded, filtered to remove noise and averaged. Three samples from the flow are taken at each sampling point shown in Fig. 4 for particle size analysis. Each test and sampling is repeated three times and the average values of the data are used for the analysis.

3.2. Hydrocyclone

A 50 mm diameter hydrocyclone (GMAX FLSmidth Krebs Hydrocyclones) is used in the experiment as the device under test. The main design parameters of the hydrocyclone are listed in Table 2 (Case 1) for geometrically similar hydrocyclones as in Fig. 1. This can be compared with other common hydrocyclone designs listed as Case 2 to Case 4 in Table 2.

3.3. Particles

Soda lime glass beads are added to the working fluid (water) to perform the experiments in the current study. The particle density is 2500 kg/m^3. A laser diffraction sensor (Sympatec GmbH, HELOS/BR) with ±1% deviation with respect to the standard meter is used for particle size distribution (PSD) analysis. The measuring zone for the insertion of wet disperses for particle size analysis varies from 0.1 μm to 875 μm.

A plot of cumulative distribution of the particles for the inlet flow sample is shown in Fig. 5 on a semi-logarithmic chart. The data for PSD is fitted using log-normal [44] andRosin–Rammler (also called Weibull distribution) [44] distributions as the uniformity of the distribution is tested with the chi-square goodness of fit test [45]. This results in confirming that the data comes from a normal distribution at the 5% significance level. Both fitted curves appropriately predict the distribution ($R^2 > 0.99$) and indicate a uniform distribution of the particles in the hydrocyclone inlet pipe. BothRosin–Rammler distribution ($R^2 = 0.9984$) and the log-normal function ($R^2 = 0.9939$) are excellent fit to the data. The particle 50% cut size (d_{50}) is 4.53 μm from the experiment, and 4.05 μm and 4.38 μm from the log-normal andRosin–Rammler distribution, respectively.

4. Results and discussion

4.1. Effect of design parameters

The ESAM described in this study relates both operating and design parameters to the Σ, which in turn is a measure of hydrocyclone performance. Hydrocyclone total length L appears directly in the equivalent area factor relation and has a linear effect on Σ. The factor β in Eq. (15) is basically a function of design parameters; but it is indirectly related to the tangential velocity through the exponent n. However, according to [40], for every hydrocyclone the tangential velocity component changes only with the radial position as the value of n is independent of the operating conditions and does not change with the vertical position. Thus, β is considered a design parameter and evaluating the β factor can be useful in comparing different designs.

Table 2
Hydrocyclone geometric parameters; dimensions are defined in Fig. 1.

Case	Parameter	D_i/D	D_o/D	L/D	L_1/D	l	θ (°)
1	Current study	0.44	0.24	17.8	1.24	0.84	–
2	Rietema	0.28	0.34	5	–	0.4	20
3	Demco 4H	0.26	0.33	3.3	0.55	0.55	18
4	Bradley	1/7	1/5	–	1/2	1/3	9

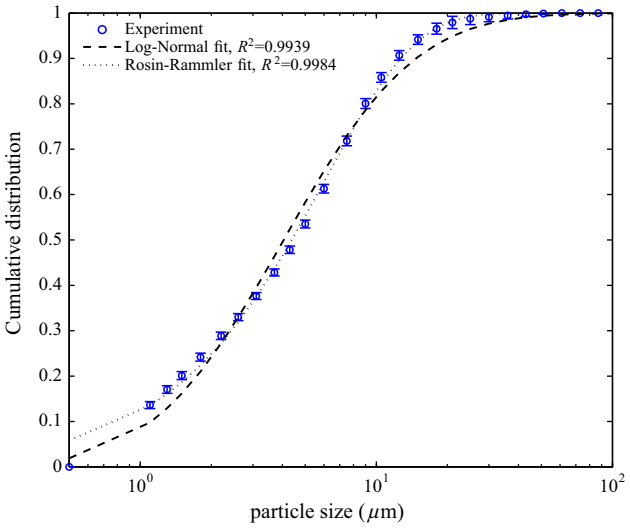

Fig. 5. Particle size distribution for the particles in the current study with error bars (d_{50} = 4.53 μm) and the log-normal fit (d_{50} = 4.05 μm) and Rosin–Rammler fit (d_{50} = 4.38 μm).

The different values for n reported in the literature are discussed in [40] where the method of measurement is described. This exponent for different designs is found to typically be between 0.7 and 0.9 [46]. An average value of 0.8 is suggested for hydrocyclones [39,47] and this value is used for further investigation in the current study.

Values of β for different D_o/D and D_i/D are obtained from Eq. (15) and are plotted in Figs. 6 and 7 for two different values of n. These figures show that β increases with either increasing the ratio of the inlet diameter or the overflow diameter to the hydrocyclone diameter. The maximum value of β is obtained for large inlet and overflow outlet diameter. Comparing the two figures shows that increasing the value of n decreases the β value. Also, β values according to Figs. 6 and 7 can change from about 0.05 for small diameters to about 5 for large inlet and overflow diameter. However, the condition $(2D_i/D + D_o/D) \leq 1$ restricts this diameters. This limit $(2D_i/D + D_o/D = 1)$ is shown by a dotted line on Figs. 6 and 7. The shaded areas above the dotted lines are where the inlet flow stream collides with the vortex finder wall and hence such diameters of the inlet and vortex finder should be avoided due to creating turbulence to the inlet flow stream. Thus, the values of β cannot exceed 2 (for $n = 0.7$) and 1.9 (for $n = 0.9$) for the diameter ranges shown in the figures for hydrocyclones mentioned above.

For a constant pressure drop, increasing the β results in a higher Σ and thus a smaller particle cut size according to Eq. (12). However, in most applications, changing in the inlet and/or the outlet diameters changes the pressure drop, which affects the performance of the device. Increasing the equivalent settling area of a hydrocyclone by increasing the overflow diameter is a better choice than increasing the inlet diameter because the equivalent area is more sensitive to the overflow diameter. This can be quan-

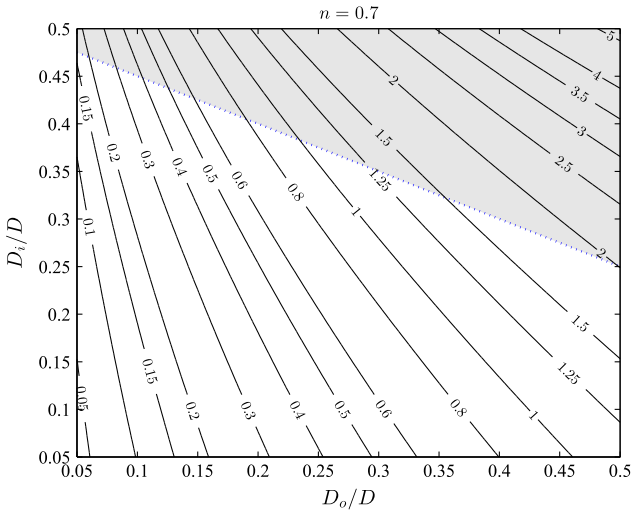

Fig. 6. Contours of β for different values of D_i/D and D_o/D ($n = 0.7$); dotted line is where $2D_i/D + D_o/D = 1$; shaded area is where $2D_i/D + D_o/D > 1$.

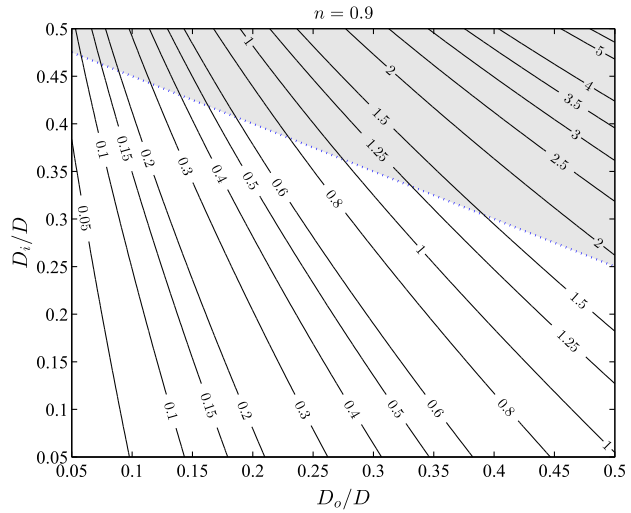

Fig. 7. Contours of β for different values of D_i/D and D_o/D ($n = 0.9$); dotted line is where $2D_i/D + D_o/D = 1$; shaded area is where $2D_i/D + D_o/D > 1$.

tified by calculating the partial derivatives of β in terms of D_i/D or D_o/D. as in Eqs. (16) and (17).

$$\frac{\partial\beta}{\partial(D_i/D)} = \frac{\pi n(2n+1)[1-(D_o/D)^2]}{[(D/D_o)^{2n}-1](1-D_i/D)^{2n+2}} \tag{16}$$

$$\frac{\partial\beta}{\partial(D_o/D)} = \frac{2\pi n(1-D_i/D)^{-2n-1}}{(D/D_o)^{2n}-1}\left[\frac{n\left[1-(D_o/D)^2\right](D/D_o)^{2n+1}}{(D/D_o)^{2n}-1} - \frac{D_o}{D}\right] \tag{17}$$

The plots of the partial derivatives of β (sensitivity) in terms of D_i/D (D_o/D remains constant) and D_o/D (D_i/D remains constant) are shown in Fig. 8 for $n = 0.7$ and in Fig. 9 for $n = 0.9$ at three constant values of 0.1, 0.2 and 0.4 for D_i/D (or D_o/D). Changes in β as a result of changes in D_o/D (at a constant D_i/D) are greater than the changes in D_i/D changes (at a constant D_o/D). Since the appearance of the overflow diameter D_o in the β relation is due to the pressure drop, changing the pressure drop has more effect on β and the tangential

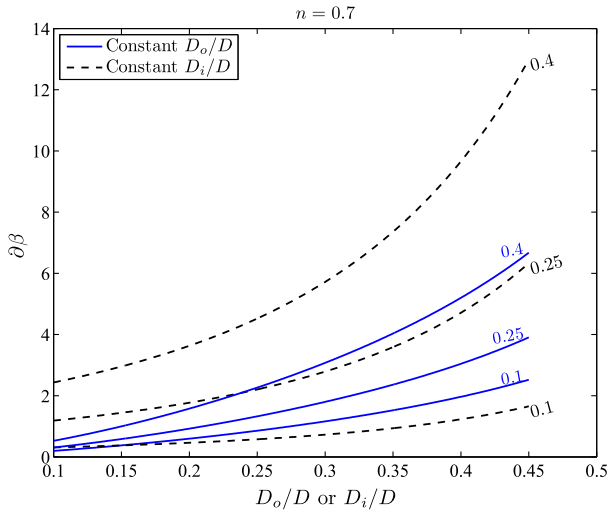

Fig. 8. $\partial\beta/\partial(D_i/D)$ and $\partial\beta/\partial(D_o/D)$ for different values of D_i/D and D_o/D ($n = 0.7$).

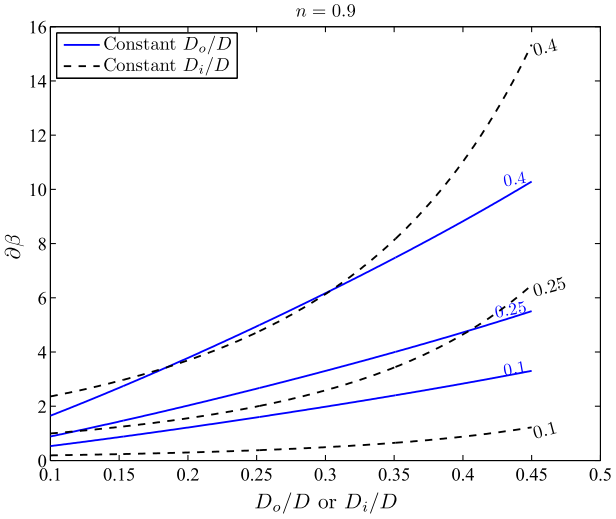

Fig. 9. $\partial\beta/\partial(D_i/D)$ and $\partial\beta/\partial(D_o/D)$ for different values of D_i/D and D_o/D ($n = 0.9$).

velocity than changing the inlet diameter and keeping the pressure drop constant.

Comparing Figs. 8 and 9 shows that increasing the value of n results in increasing the slope of β with respect to D_i/D or D_o/D. These changes for overflow diameter are greater than the inlet diameter ratio and particularly for higher values of the overflow diameters.

4.2. Model validation

The experimental results are used to validate the ESAM. To do this, the Σ values are calculated from ESAM (Σ_{model}) with the average chosen value of $n = 0.8$. These are plotted versus experimental values obtained from the experimental data (Σ_{exp}) for the current study. Values of Σ_{model} and Σ_{exp} are also calculated for other types of the hydrocyclones (Case 2, 3 and 4 in Table 2) assuming similar hydrocyclone diameter of 50 mm as in the hydrocyclone in the current study. The design parameters for these designs are also listed in Table 2.

To obtain the equivalent area factor from the experiments (Σ_{exp}) the underflow cut size at each test is determined by particle size analysis using the same method previously explained for the inlet

flow particles. For the underflow cut size diameter Eq. (6) is used to calculate the settling velocity under gravitational acceleration. At each operating condition (constant flow rates and pressure drop) for a certain inlet flow rate, Σ_{exp} is calculated from Eq. (12). For Rietema, Demco 4H and Bradley hydrocyclone designs, the values of Σ_{exp} are obtained from the experimental correlations in [15] by calculating the flow rate and cut size at similar pressure drops as in the current study. Pressure drop is calculated from the difference between the inlet and the underflow pressure.

The equivalent area factor from the ESAM (Σ_{model}) is calculated from Eq. (14) at each inlet flow rate for all designs. As pressure drop is required for obtaining Σ_{model} and to be able to compare the results of the experiment and the model, the same experimental pressure drop is used.

The plots of Σ_{exp} and Σ_{model} ($n = 0.8$) resulted from the calculations for the current study (and for Rietema, Demco 4H and Bradley hydrocyclones) are shown in part (a) of Figs. 10–12. As can be seen from the figures, there is a discrepancy between the experimental data and the data predicted using the proposed $n = 0.8$. This is particularly noticeable for the Bradley hydrocyclone which using $n = 0.8$ leads to underestimated values of the equivalent area factor. To obtain the best match between the experiment and the ESAM results, the sum of squared errors (SSE) between the values of Σ_{model} and Σ_{exp} in each hydrocyclone is minimized by examining the exponent n). The resulted exponent after minimizing SSE is called the *predicted n* and is represented by n_p. The results of comparing the equivalent area factor between the ESAM and experiment using n_p are plotted as part (b) of Figs. 10–12. Points on the 45° line indicate an exact match between ESAM and experiment. The lines of ±15% deviation from the best match are also plotted in the figure. The comparison in Fig. 10 shows a good agreement between the ESAM and experiment within 15%.

As can be seen from Fig. 10, the exponent n_p for the current study is 0.88, which is comparable with the value of 0.8 for n suggested in [39]. The obtained value of n_p is 0.94 for Rietema hydrocyclone, 0.88 for Demco 4H hydrocyclone and 0.31 for Bradley hydrocyclone shown in Figs. 11(b), 12(b) and 13(b), respectively. The values obtained from the ESAM as determined above, are close to the chosen value of $n = 0.8$ except for the Bradley hydrocyclone that there is a significant discrepancy between the two exponents.

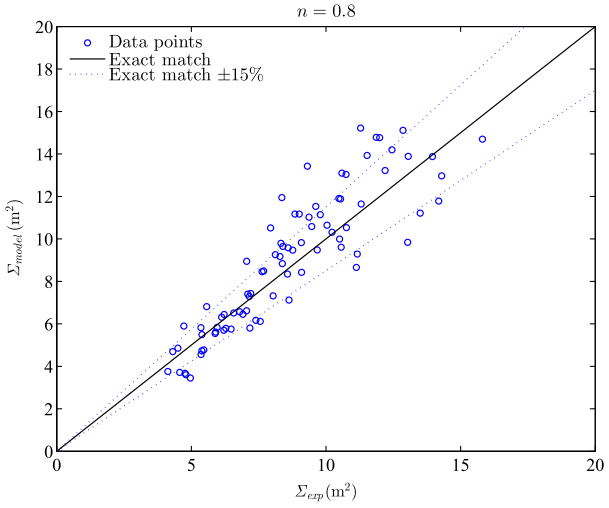

(a) Experimental data and model prediction

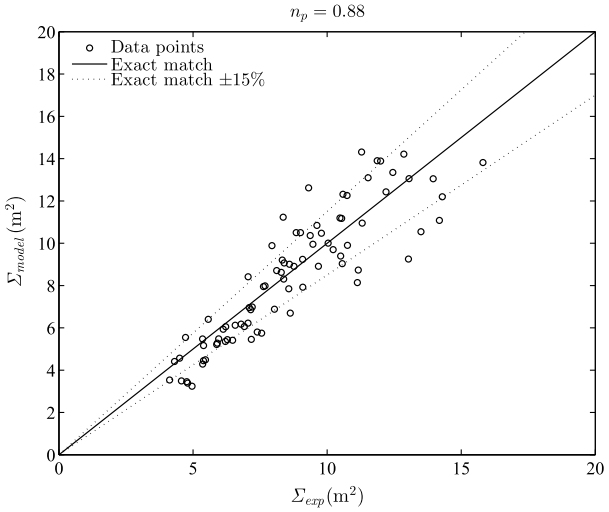

(b) Adjusted model to fit the experimental data

Fig. 10. Experimental equivalent area factor vs. ESAM for the data of the current study; (a) $n = 0.8$ and (b) $n_p = 0.88$.

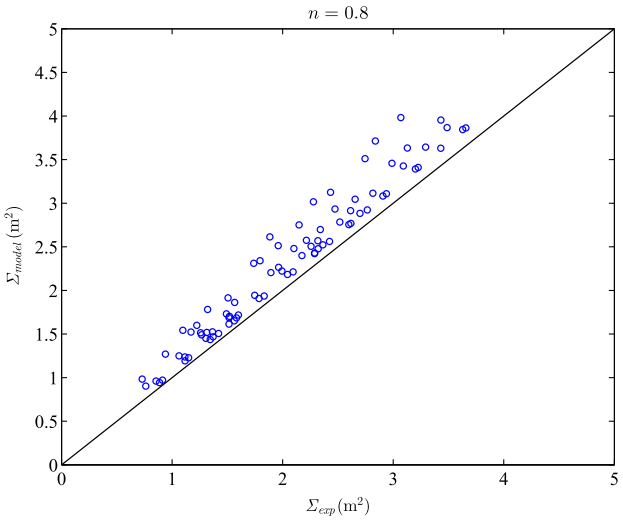

(a) Experimental data and model prediction

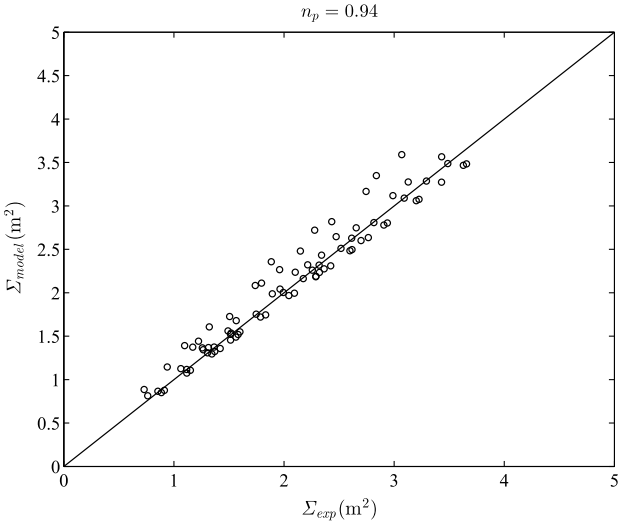

(b) Adjusted model to fit the experimental data

Fig. 11. Experimental equivalent area factor vs. ESAM for similar pressure drops and inlet concentrations as in the current study for Rietema hydrocyclone; (a) $n = 0.8$ and (b) $n_p = 0.94$; experimental value for Rietema hydrocyclone is from the correlations in [15].

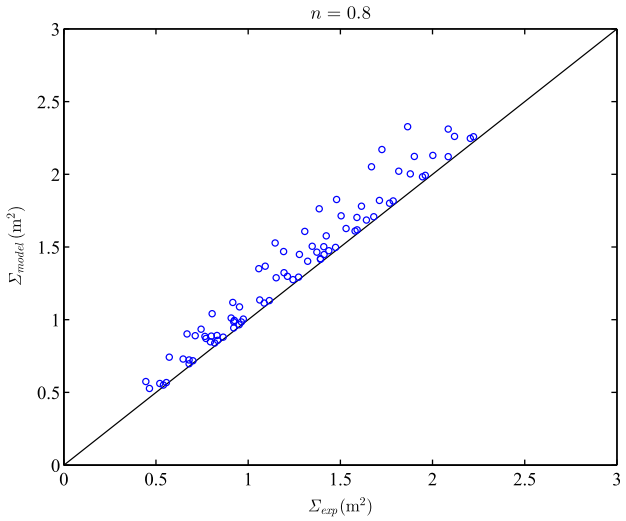

(a) Experimental data and model prediction

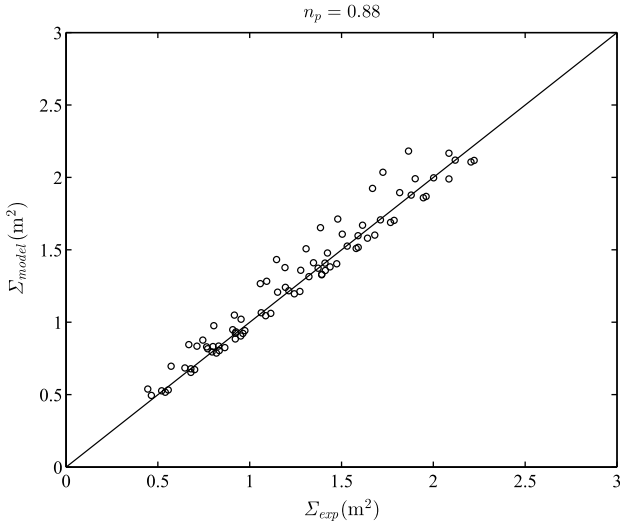

(b) Adjusted model to fit the experimental data

Fig. 12. Experimental equivalent area factor vs. ESAM for similar pressure drops and inlet concentrations as in the current study for Demco 4H hydrocyclone; (a) $n = 0.8$ and (b) $n_p = 0.88$; experimental value for Demco 4H hydrocyclone is from the correlations in [15].

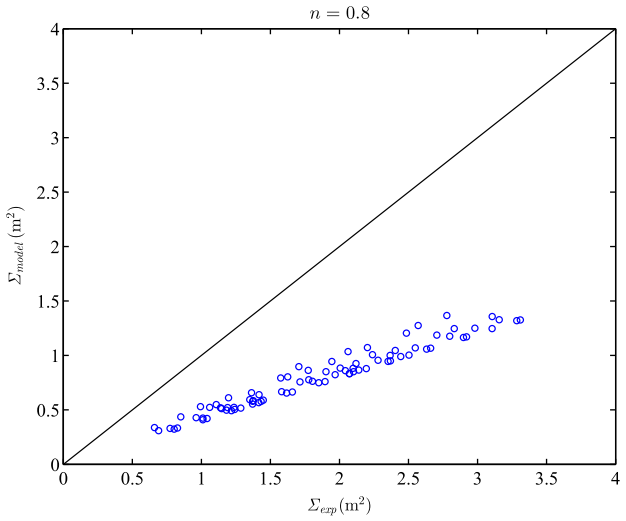

(a) Experimental data and model prediction

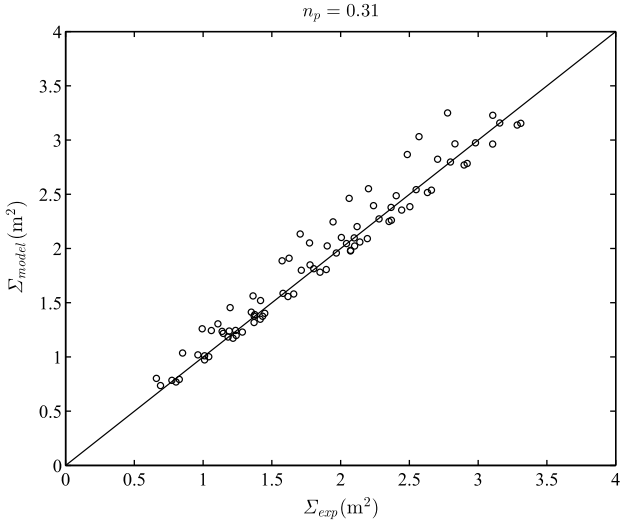

(b) Adjusted model to fit the experimental data

Fig. 13. Experimental equivalent area factor vs. ESAM for similar pressure drops and inlet concentrations as in the current study for Bradley hydrocyclone; (a) $n = 0.8$ and (b) $n_p = 0.31$; experimental value for Bradley hydrocyclone is from the correlations in [15].

Comparing the design parameters for different hydrocyclones in Table 2, it is observed that the cone angle is noticeably different between Bradley, Rietema and Demco 4H hydrocyclones. This angle along with other design parameters is expected to affect the value of n. This results in a discrepancy between the model and experiments for a Bradley hydrocyclone shown in Fig. 13(a) since a constant $n = 0.8$ is used for all the hydrocyclone types.

To investigate the discrepancy between the ESAM prediction and experimental equivalent area factor observed for the Bradley hydrocyclone, the values of exponent n are compared with the literature. To do this, the experimentally obtained n for Bradley hydrocyclones are extracted from [40] and compared to the predicted values of n_p from the ESAM (predicted exponent for the best match between Σ_{model} and Σ_{exp}). The tests conditions and the results of the comparison are summarized in Table 3. The values in Table 3 indicate that the predicted exponents n_p from ESAM are in good agreement with the values of n measured experimentally with maximum deviation of 0.06. This denotes that the ESAM can be confidently used to approximate the n and hence Σ. Know-

Table 3
Comparing the experimental value of the tangential velocity exponent n [40] and the predicted values using the ESAM (n_p); $D_i/D = 1/7.5, D_o/D = 1/5; D_u/D = 1/15, \theta = 9^\circ$ (dimensions are defined in Fig. 1).

D (mm)	Pressure drop (kPa)	Inlet flow rate (m^3/h)	n (experiment)	n_p (ESAM)
15	46.9	0.072	0.11	0.16
15	81.4	0.091	0.15	0.16
15	146.9	0.114	0.16	0.17
15	193.7	0.112	0.18	0.17
15	242.0	0.128	0.19	0.17
75	30.3	1.363	0.17	0.19
75	31.7	1.363	0.16	0.19
75	84.8	2.066	0.19	0.20
75	86.9	2.066	0.19	0.20
75	84.1	2.066	0.18	0.20
75	85.5	2.066	0.19	0.20
75	134.4	2.495	0.24	0.20
75	135.8	2.495	0.24	0.20
75	206.8	2.971	0.26	0.20

ing this the discrepancy in Σ values between the ESAM and experiment is attributed to the value of n used in the ESAM to predict the Σ in Bradley hydrocyclone. It shows that despite the generally accepted range for exponent n (0.7–0.9 [46] or 0.5–0.9 [34]), for particular designs this may decrease to a small value such as 0.2. Therefore, the recommended average 0.8 value for n [47,39] that is used in the model may not fit all hydrocyclone designs. The best value of n that fits the model for each design geometry should be obtained from the experimental results.

To evaluate the effect of design parameters on the equivalent area factor, plots of Σ as a function of pressure drop (according to Eq. (15)) are shown in Fig. 14 for the four types of hydrocyclones. Each plot compares the data of experimental Σ and the curve fitted to the data with Σ from the ESAM ($n = 0.8$). This comparison has the advantage of including the effect of hydrocyclone total length L (see Fig. 1) which does not appear in β. From Fig. 14 it can be concluded that there is a good agreement between the ESAM and the experimental results. This shows that the proposed ESAM in Eq. (14) predicts well the effect of the design parameters on Σ. As discussed above, the discrepancy between the ESAM and the experimental points for the Bradley hydrocyclones is attributed to the specifications of this hydrocyclone that requires a smaller value of n to predict the tangential velocity profile.

4.3. Predicting the tangential velocity profile

Estimating the value of n for a hydrocyclone without needing velocimetry is an important aspect of the ESAM. Using the estimated value of n, the tangential velocity profile can also be predicted. Typically to determine the tangential velocity profile measuring of the velocity components is required [48,7]. Velocimetery measurement in a hydrocyclone is difficult as a result of complicated flow geometry. In addition, some measurement techniques are invasive and some are difficult to perform in an industrial setting. Thus, an alternate method of determining the tangential velocity component (the most important velocity component affects the separation performance [7]) can be useful.

The following procedure is proposed as an alternative method of determining the tangential velocity profile in hydrocyclones on the basis of the ESAM:

1. Experimentally determine the flow rate, fluid properties (density and viscosity), particle density and the separation cut size (using a particle size analysis method).
2. From the information obtained in step 1, settling velocity is determined from Eq. (6).
3. The experimental equivalent area factor is calculated from Eq. (12).

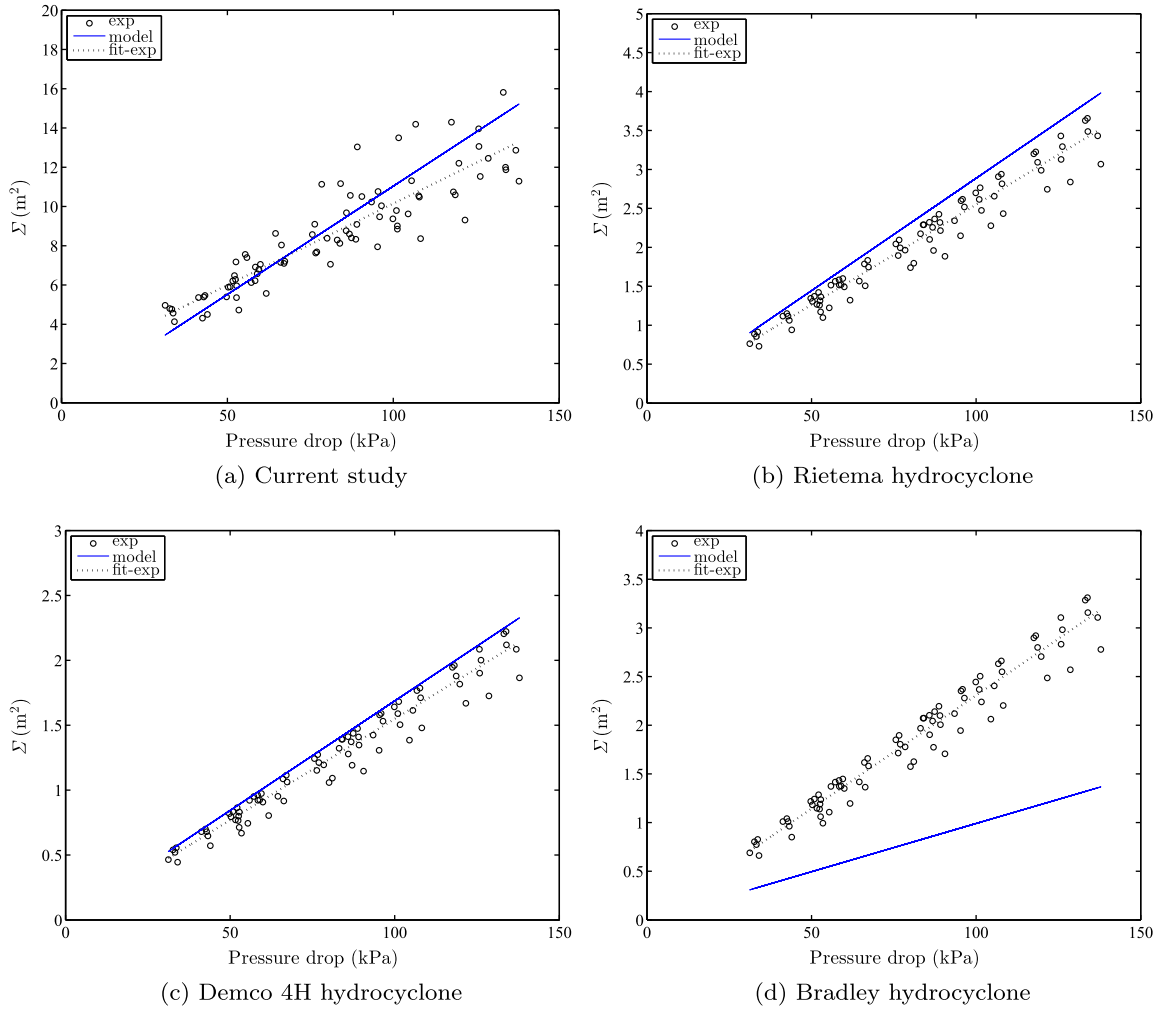

Fig. 14. Comparing the experimental equivalent area factor vs. pressure drops with the values predicted with ESAM for similar pressure drops and inlet concentrations as in the current study; (a)–(d): $n = 0.8$; experimental value for Rietema, Demco 4H and Bradley hydrocyclones are based on correlations in [15].

4. Equating this value with Eq. (14) at a known pressure drop gives the value of n.
5. Then v_θ is calculated using Eq. (7) using n at the known flow rate and inlet section dimensions.

Following these steps the velocity profiles for the tangential velocity in four hydrocyclone cases is obtained. Fig. 15 shows the normalized tangential velocity (normalized with inlet velocity) at different normalized radiuses (the radial distance from the hydrocyclone centerline). Higher values of the v_θ/v_{inlet} is obtained for Rietema and Demco 4H hydrocyclones. This is interesting as the maximum equivalent area factor is observed in the hydrocyclone Case 1 (compare Figs. 10–12) shows that the effects of the other design and operational parameters on the separation performance may be more significant that the centrifugal acceleration.

Experimental data from [5] is used to examine the proposed method of tangential velocity profile prediction according to the above mentioned procedure. The hydrocyclone dimensions and test conditions are listed in Table 4. The value of exponent n_p is obtained by determining Σ_{model} and Σ_{exp}. Assuming that the liquid density equals 1000 kg/m^3 and using ESAM Σ_{model} is determined. The experimental test in [5] had no solid particles and performed only for velocity measurements. Thus, Σ_{exp} for the test in [5] is calculated using the correlations developed in [15] assuming sand particles with $\Delta\rho = 1650$ kg/m^3, water as liquid with $\mu = 1$ mPa.s and low particle volume concentration as 0.05%. Equating these two equivalent area factors for the model and experiment results in $n_p = 0.41$. Using this predicted exponent and approximating the rectangular inlet pipe depth H from the equivalent area of the inlet circular pipe, v_θ is obtained using Eq. (7). This predicted tangential velocity is compared to the experimental data [5] in Fig. 16. The comparison shows a good agreement between the predicted values and the experimental data with more discrepancies for smaller radiuses. The predicted velocity profile is $v_\theta = 0.31/r^{0.41}$ and the profile resulted from the experimental data is $v_\theta = 0.25/r^{0.51}$ which show a difference of 0.1 between the exponents and 0.06 between the constants. This results in a maximum error of 22.7% at $r = 0.0035$ m at the maximum tangential velocity as shown in Fig. 16.

Employing this technique, information at a single data point can be used to estimate the velocity profile. However, having more experimental data points at different operating conditions results in a more accurate estimation of n by minimizing the sum of squared errors of prediction. Most of the measurements for the tangential velocity component are in pure water or lightly seeded water [5–7,10] as the measurements are simpler to perform. However, these experiments do not replicate the real applications of the hydrocyclones in terms of the effects of particles on the tangential velocity component. Predicting the tangential velocity profile on the basis of the proposed method in this study do not required velocity measurement and is based on the experimental cut size.

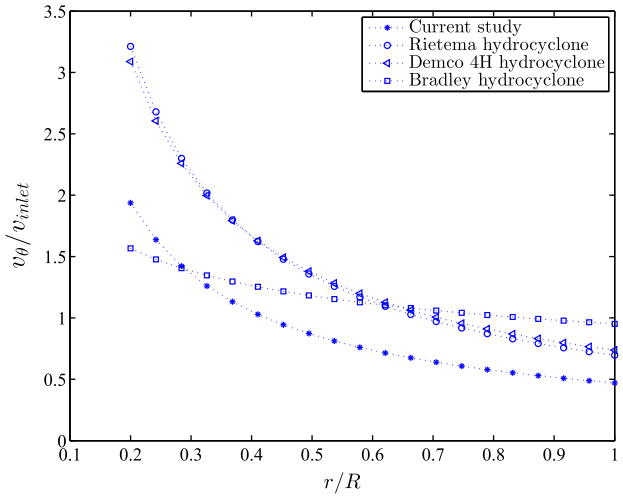

Fig. 15. Normalized tangential velocity profiles at separation zone vs. normalized radius for different hydrocyclones ($R = D/2$).

Table 4
Hydrocyclone geometric parameters and experiment conditions for examining the tangential velocity profile; dimensions are defined in Fig. 1.

Parameter	Value
D (mm)	75
D_i (mm)	0.28D
D_o (mm)	0.34D
D_u (mm)	0.16D
L (mm)	5D
l (mm)	0.4D
ΔP (kPa)	25
Q (m^3/h)	1.82

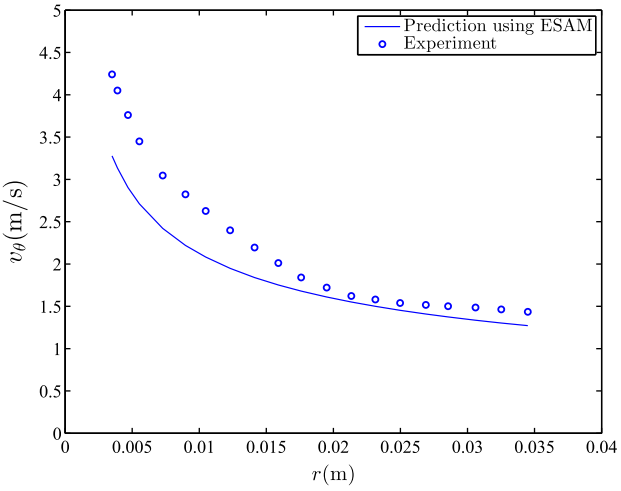

Fig. 16. Comparison of predicted tangential velocity profiles vs. hydrocyclone radius (r) at separation zone and experimental data from [5] for test conditions as in Table 4; $R^2 = 0.71$.

5. Conclusions

A mathematical model has been developed to predict the equivalent settling area factor in hydrocyclones (ESAM) and it has been validated using data from an experimental study. The experimental results are in good agreement with the ESAM prediction. ESAM can be used to predict the equivalent area factor for a variety of hydrocyclone designs. The equivalent area factor Σ can also be used to compare other centrifugal separators and a continuous settling tank to provide insight into the relative performance of different centrifugal separation techniques. The effects of hydrocyclone inlet and overflow diameters are studied. Σ in hydrocyclones is increased by increasing either the hydrocyclone inlet diameter or the overflow diameter, but it is more sensitive to the overflow diameter.

Since the model development basis is the centrifugal acceleration, the ESAM together with the experimental equivalent area obtained from performance experiments can be used to predict the tangential velocity profile in the hydrocyclone. This prediction is validated by comparison of the tangential velocity profile of a given hydrocyclone. This method has the benefit of predicting

the tangential velocity profile without requiring complex and expensive instruments for velocimetry measurement.

The average value of 0.8 is suggested in the literature for the exponent n in the tangential velocity profile function for hydrocyclones. It is shown that the value of this exponent is significantly geometry dependent. For three of the hydrocyclone designs studied in this paper, the exponent values are close to the average, while for Bradley hydrocyclone n is found to be 0.31. The proper exponent for each hydrocyclone design can be determined from the ESAM by comparing with experimental data and the ESAM can now be used as a design tool for hydrocyclones.

Acknowledgments

The authors acknowledge the supports from Natural Sciences and Engineering Research Council of Canada (NSERC) and Canada Foundation for Innovation (CFI).

References

[1] H. Anlauf, Recent developments in centrifuge technology, Sep. Purif. Technol. 58 (2) (2007) 242–246, http://dx.doi.org/10.1016/j.seppur.2007.05.012.
[2] U. Schaflinger, Review article centrifugal separation of a mixture, Fluid Dyn. Res. 6 (1990) 213–249.
[3] C.M. Ambler, The evaluation of centrifuge performance, Chem. Eng. Prog. 48 (3) (1952) 150–158.
[4] C.M. Ambler, The theory of scaling up laboratory data for the sedimentation type centrifuge, J. Biochem. Microbiol. Technol. Eng. 1 (2) (1959) 185–205, http://dx.doi.org/10.1002/jbmte.390010206.
[5] B. Dabir, C.A. Petty, Measurements of mean velocity profiles in a hydrocyclone using laser Doppler anemometry, Chem. Eng. Commun. 48 (1986) 377–388, http://dx.doi.org/10.1080/00986448608910025.
[6] Q. Zhao, G. Xia, A theoretical model for calculating pressure drop in the cone area of light dispersion hydrocyclones, Chem. Eng. J. 117 (3) (2006) 231–238, http://dx.doi.org/10.1016/j.cej.2005.11.012.
[7] J. Bergstrom, H. Vomhoff, Experimental hydrocyclone flow field studies, Sep. Purif. Technol. 53 (1) (2007) 8–20, http://dx.doi.org/10.1016/j.seppur.2006.09.019.
[8] M. Brennan, M. Narasimha, P. Holtham, Multiphase modelling of hydrocyclones prediction of cut-size, Miner. Eng. 20 (4) (2007) 395–406, http://dx.doi.org/10.1016/j.mineng.2006.10.010.
[9] L. Marins, D. Duarte, J. Loureiro, C. Moraes, a.S. Freire, LDA and PIV characterization of the flow in a hydrocyclone without an air-core, J. Petrol. Sci. Eng. 70 (3–4) (2009) 168–176, http://dx.doi.org/10.1016/j.petrol.2009.11.006.
[10] Y. Liu, Q. Yang, P. Qian, H.-l. Wang, Experimental study of circulation flow in a light dispersion hydrocyclone, Sep. Purif. Technol. 137 (2014) 66–73, http://dx.doi.org/10.1016/j.seppur.2014.09.020.
[11] D. Bradley, A theoretical study of the hydraulic cyclone, Ind. Chem. 34 (1958) 473–480.
[12] K. Rietema, Performance and design of hydrocyclones-III, Chem. Eng. Sci. 15 (3–4) (1961) 310–319, http://dx.doi.org/10.1016/0009-2509(61)85035-5.
[13] C.C. Hwang, H.Q. Shen, G. Zhu, M.M. Khonsari, On the main flow pattern in hydrocyclones, J. Fluids Eng. 115 (March) (1993) 21–25, http://dx.doi.org/10.1115/1.2910106.
[14] L. Castilho, R. Medronho, A simple procedure for design and performance prediction of Bradley and Rietema hydrocyclones, Miner. Eng. 13 (2) (2000) 183–191.
[15] M. Coelho, R. Medronho, A model for performance prediction of hydrocyclones, Chem. Eng. J. 84 (1) (2001) 7–14, http://dx.doi.org/10.1016/S1385-8947(00)00265-5.
[16] K. Nageswararao, D. Wiseman, T. Napier-Munn, Two empirical hydrocyclone models revisited, Miner. Eng. 17 (5) (2004) 671–687, http://dx.doi.org/10.1016/j.mineng.2004.01.017.
[17] T. Neesse, J. Dueck, Dynamic modelling of the hydrocyclone, Miner. Eng. 20 (4) (2007) 380–386, http://dx.doi.org/10.1016/j.mineng.2006.11.004.
[18] E. Donskoi, S. Suthers, J. Campbell, T. Raynlyn, Modelling and optimization of hydrocyclone for iron ore fines beneficiation using optical image analysis and iron ore texture classification, Int. J. Miner. Process. 87 (3–4) (2008) 106–119, http://dx.doi.org/10.1016/j.minpro.2008.02.006.
[19] S. Amini, D. Mowla, M. Golkar, F. Esmaeilzadeh, Mathematical modelling of a hydrocyclone for the down-hole oil-water separation (DOWS), Chem. Eng. Res. Des. 90 (12) (2012) 2186–2195, http://dx.doi.org/10.1016/j.cherd.2012.05.007.
[20] J. Dueck, M. Farghaly, T. Neesse, The theoretical partition curve of the hydrocyclone, Miner. Eng. 62 (2014) 25–30, http://dx.doi.org/10.1016/j.mineng.2013.10.004.
[21] L. Plitt, A mathematical model of the hydrocyclone classifier, CIM Bull. 69 (776) (1976) 114–123.
[22] W. Kraipech, W. Chen, T. Dyakowski, A. Nowakowski, The performance of the empirical models on industrial hydrocyclone design, Int. J. Miner. Process. 80 (2-4) (2006) 100–115, http://dx.doi.org/10.1016/j.minpro.2005.02.005.
[23] J. Severino, L. Gomez, S. Wang, R. Mohan, O. Shoham, Mechanistic modeling of solids separation in solid/liquid hydrocyclones, in: Proceedings of SPE Annual Technical Conference and Exhibition, Society of Petroleum Engineers, 2009, pp. 4–9. doi:10.2118/124499-MS.
[24] M. Narasimha, M. Brennan, P.N. Holtham, A review of CFD modelling for performance predictions of hydrocyclone, Eng. Appl. Comput. Fluid Mech. 1 (2) (2007) 109–125.
[25] Q. Yang, H.-l. Wang, Y. Liu, Z.-m. Li, Solid/liquid separation performance of hydrocyclones with different cone combinations, Sep. Purif. Technol. 74 (3) (2010) 271–279, http://dx.doi.org/10.1016/j.seppur.2010.06.014.
[26] M. Ghadirian, R.E. Hayes, J. Mmbaga, A. Afacan, Z. Xu, On the simulation of hydrocyclones using CFD, Can. J. Chem. Eng. 91 (May) (2013) 950–958, http://dx.doi.org/10.1002/cjce.21705.
[27] N. Chakraborti, J.D. Miller, Fluid flow in hydrocyclones: a critical review, Miner. Process. Extr. Metall. Rev. 11 (1992) 211–244.
[28] M. Narasimha, M.S. Brennan, P.N. Holtham, A review of flow modeling for dense medium cyclones, Coal Preparat. 26 (2) (2006) 55–89, http://dx.doi.org/10.1080/07349340600619733.
[29] F. Concha, Flow pattern in hydrocyclones, Kona-Powder Part. 25 (25) (2007) 97–132, http://dx.doi.org/10.14356/kona.2007011.
[30] Z. Berk, Centrifugation, in: Food Process Engineering and Technology, Elsevier Inc., 2009, pp. 217–232.
[31] L. Svarovsky, Solid/Liquid Separation, fourth ed., Butterworth-Heinemann, 2000.
[32] R. Sabbagh, M.G. Lipsett, C.R. Koch, D.S. Nobes, Hydrocyclone performance and energy consumption prediction: a comparison with other centrifugal separators, Sep. Sci. Technol. 50 (6) (2015) 788–801, http://dx.doi.org/10.1080/01496395.2014.978463.
[33] R. Sabbagh, M.G. Lipsett, C.R. Koch, D.S. Nobes, Theoretical and experimental study of hydrocyclone performance and equivalent settling area, in: ASME 20 14 International Congress and Exposition IMECE2014, ASME, Montreal, Quebec, Canada. http://dx.doi.org/10.1115/IMECE2014-37482.
[34] L. Svarovsky, Hydrocyclones, Holt, Rinehart and Winston LTD, London, UK, 1984.
[35] R.L. Panton, Incompressible Flow, fourth ed., John Wiley & Sons, Inc. All, 2013.
[36] K. Rietema, Performance and design of hydrocyclones-II, Chem. Eng. Sci. 15 (3–4) (1961) 298–302.
[37] D. Kelsall, A further study of the hydraulic cyclone, Chem. Eng. Sci. 2 (1953) 254–272.
[38] M.J. Fisher, R.D. Flack, Velocity distributions in a hydrocyclone separator, Exp. Fluids 32 (2002) 302–312, http://dx.doi.org/10.1007/s003480100344.
[39] T. Neesse, J. Dueck, Air core formation in the hydrocyclone, Miner. Eng. 20 (2007) 349–354, http://dx.doi.org/10.1016/j.mineng.2007.01.007.
[40] D. Bradley, The Hydrocyclone, Pergamon Press Ltd., 1965.
[41] J. Richardson, W. Zaki, Sedimentation and fluidisation: part i, Chem. Eng. Res. Des. 75 (3) (1997) S82–S100, http://dx.doi.org/10.1016/S0263-8762(97)80006-8.
[42] A. Zeidan, S. Rohani, A. Bassi, P. Whiting, Review and comparison of solids settling velocity models, Rev. Chem. Eng. 19 (5) (2003) 473–530, http://dx.doi.org/10.1515/REVCE.2003.19.5.473.
[43] Standard practice for static calibration of electronic transducer-based pressure measurement systems for geotechnical purposes; ASTM Standard D5720-95, ASTM International, West Conshohocken, PA, 2002, http://dx.doi.org/10.1520/D5720-95R09.2.
[44] A.C. Hoffmann, L.E. Stein, Gas Cyclones and Swirl Tubes, second ed., Springer, Berlin, 2008.
[45] T.T. Soong, Fundamentals of Probability and Statistics for Engineers, John Wiley & Sons Ltd, West Sussex, England, 2004.
[46] C.T. Crowe, Mutiphase Flow Handbook, CRC Press, Boca Raton, USA, 2006.
[47] D. Bradley, D.J. Pulling, Flow patterns in the hydraulic cyclone and their interpretation, Trans. Inst. Chem. Eng. 37 (1959) 34–45.
[48] K.D. Jensen, Flow measurements techniques, J. Braz. Soc. Mech. Sci. Eng. XXVI (4) (2004) 400–419.